LANGMUIR

pubs.acs.org/Langmuir Article

Highly Conductive and Mechanically Robust Cellulose Hydrogels Enabled by Attapulgite-Derived Titanium Silicate

Miaomiao Wu, Hu Liu, Xiong-Fei Zhang,* Mengjie Li, and Jianfeng Yao*

Cite This: https://doi.org/10.1021/acs.langmuir.5c02530 Read Online

ACCESS | Metrics & More | Article Recommendations | Supporting Information

ABSTRACT: The development of cellulose-based hydrogels with integrated mechanical robustness, ionic conductivity, and environmental tolerance is critical for advancing wearable electronics. Herein, we report a dual-cross-linked cellulose hydrogel reinforced with attapulgite-derived titanium silicate (ATS). An acid-hydrothermal approach was used to transform attapulgite into ATS. ATS has a porous structure with uniform channels, and it can serve as a physical cross-linker to improve the mechanical robustness of the hydrogel. The as-prepared hydrogel demonstrated a high tensile strength (155 kPa), fracture elongation (177%), and compressive stress (0.58 MPa). Simultaneously, the ATS-engineered porous network facilitates rapid ion transport, yielding a high ionic conductivity of 2.45 S m^{-1}. When assembled into a strain sensor, the hydrogel can realize the precise detection of human motions. This work provides a sustainable strategy for designing sensors through inorganic filler engineering to tune the mechanical and conductive properties of hydrogels.

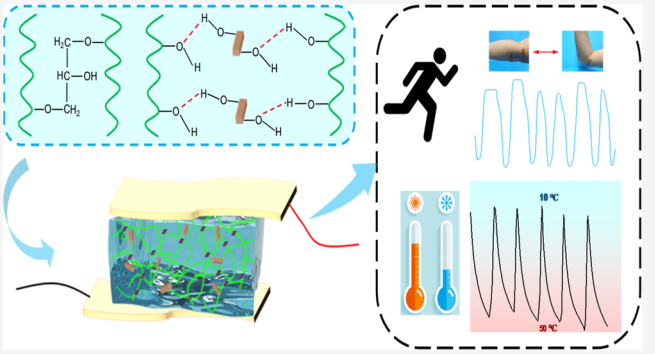

INTRODUCTION

Recently, flexible electronics have garnered significant attention for their potential in healthcare monitoring,[1] human−machine interfaces,[2] and wearable devices.[3,4] These applications demand materials that combine mechanical robustness, environmental tolerance, and high ionic conductivity.[5,6] Owing to their three-dimensional polymeric networks and tunable physicochemical properties, hydrogels are promising candidates for such devices.[7,8] While synthetic polymer-based hydrogels (e.g., polyacrylamide or poly(acrylic acid)) dominate current studies, growing environmental concerns and the demand for biocompatibility have shifted focus toward natural polymers that align with sustainable development goals.[9,10] Among natural polymers, cellulose stands out because of its abundance, biocompatibility, and sustainability.[11,12] However, conventional cellulose hydrogels often suffer from inherent limitations, including weak mechanical strength, insufficient ionic conductivity, and poor structural stability under extreme conditions, which hinder their practical utility in advanced sensing systems.[13,14]

Previous studies have explored diverse strategies to enhance the mechanical and conductive properties of cellulose hydrogels, such as the introduction of inorganic fillers (e.g., natural clays or carbon-based materials) or chemical cross-linkers (e.g., poly(vinyl alcohol) or starch).[15,16] Wang et al. integrated poly(vinyl alcohol) into a cellulose matrix to improve the stretchability of hydrogel sensors.[16] In addition, Prior work found that MXene-reinforced cellulose hydrogels exhibited superior strain sensing performance, with a gauge factor of 1.18 and stability over 2000 cycles, demonstrating their potential for motion detection.[17] By exploiting bentonite-cellulose coordination, Wang et al. developed an all-natural hydrogel that exhibited high compressive strength (3.2 MPa), ionic conductivity (89.9 mS cm^{-1}), and freezing tolerance.[18] Their work highlighted the critical role of robust interfacial bonding (e.g., Al−O−C coordination) in balancing mechanical and conductive properties. Previously, attapulgite (ATP), a natural nanorod-like silicate, was utilized to reinforce cellulose hydrogels.[19] The inherent surface hydroxyl groups (−OH) on pristine ATP facilitate strong physical interactions (e.g., hydrogen bonding) with polymer chains, promoting the formation of a secondary cross-linked network. However, native ATP exhibited a nonuniform pore distribution and limited interfacial compatibility with cellulose, resulting in inefficient stress transfer and structural instability. Addressing these structural deficiencies requires rational modification of ATP to optimize its interaction with the cellulose matrix.[20,21]

For hydrogels, recent advances highlight the importance of secondary cross-linking networks in dissipating energy and improving mechanical resilience; however, achieving a balance

Received: May 19, 2025
Revised: July 7, 2025
Accepted: July 7, 2025

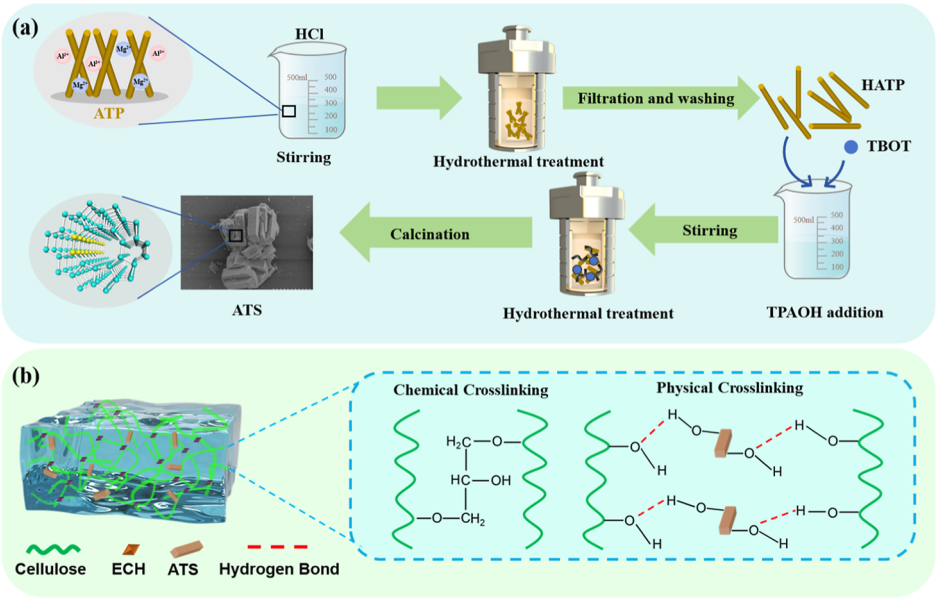

Figure 1. Schematic illustration of (a) the preparation process of ATS and (b) the dual-cross-linked ATS/cellulose hydrogels.

between high ionic conductivity and mechanical strength remains challenging.[6,22,23] This is particularly critical for sensing applications, where rapid ion transport and structural durability under repetitive deformation are essential.[24,25] In this work, a dual-cross-linked hydrogel was fabricated by combining cellulose with ATP-derived titanium silicate (ATS).[26] ATS was synthesized via acid treatment and hydrothermal crystallization of ATP, forming a hierarchical porous structure with uniform channels. ATS establishes a secondary physical network through hydrogen bonding and electrostatic interactions with cellulose chains. Moreover, epichlorohydrin (ECH) chemically cross-links the cellulose matrix to form a covalent network. This synergy enhances the mechanical strength via stress redistribution and energy dissipation while promoting ion mobility through the optimized pore structure. Furthermore, LiCl incorporation endows the hydrogel with antifreezing properties, ensuring functionality in subzero environments. The hydrogel demonstrated strain sensitivity, stability across 100 loading–unloading cycles, and reliable performance at −20 °C, validating its potential as a durable, versatile sensing material.

EXPERIMENTAL SECTION

Materials. The cellulose (cotton linter, containing ∼ 95% α-cellulose) was supplied by Nantong Cellulose Fiber Co., Ltd. (China). Prior to use, the sample was dried at 60 °C for 24 h to remove moisture. Hydrochloric acid (HCl, 36–38%) was purchased from Nanjing Chemical Reagent Co., Ltd. (Nanjing, China). Sodium hydroxide (NaOH, AR, 98%), urea (AR, 99%), and ethylene glycol (AR, 99%) were obtained from Sinopharm Chemical Reagent Co., Ltd. Epichlorohydrin (ECH) and titanium butoxide (TBOT, 98%) were acquired from Shanghai Lingfeng Chemical Reagent Co., Ltd. Tetrapropylammonium hydroxide (TPAOH, 25 wt %) was purchased from Shanghai Macklin Biochemical Technology Co., Ltd. Attapulgite (ATP), with an average diameter of 20–40 nm and a specific surface area of 140 $m^2\ g^{-1}$, was purchased from Jiuchuan Technology Co., Ltd (Jiangsu, China).

Synthesis of ATS. First, ATP (5 g) was immersed in 3.5 mol L^{-1} HCl solution (30 mL) under continuous stirring for 3 h. The mixture was then transferred into a polytetrafluoroethylene (PTFE)-lined autoclave and hydrothermally treated at 180 °C for 12 h. The resulting product was centrifugally washed with deionized water to remove residual ions, followed by vacuum drying at 100 °C for 12 h and grinding to obtain acid-treated ATP (HATP). Subsequently, 10 mL of ethylene glycol and 2 g of HATP were mixed in a beaker under vigorous stirring to form a homogeneous suspension. Then, 0.5 mL of TBOT was added, and the reaction was maintained at 110 °C with continuous stirring for 2 h, followed by heating to 165 °C for 1.5 h to complete the reaction between the silicon and titanium sources.

Afterward, 5.0 g of TPAOH was introduced into the solution, and the mixture was transferred to a PTFE autoclave for further nucleation and crystallization at 170 °C for 36 h. The solid product was collected by centrifugation, washed thoroughly with deionized water, and vacuum-dried at 100 °C for 12 h to yield the ATS precursor. Finally, the precursor was calcined in air at a heating rate of 4.0 °C min^{-1} to 550 °C and held for 5 h to remove organic templates, resulting in crystalline ATS.

Preparation of Hydrogels. The NaOH/urea solution was used for cellulose dissolution. An aqueous solution containing 7 wt % NaOH and 12 wt % urea (19.4 g) was precooled at −20 °C for 1 h. Subsequently, 0.6 g of cotton linter was added to the solution under vigorous stirring for 30 min to form a homogeneous cellulose solution. Predetermined amounts of ATS particles (0, 0.03, 0.06, or 0.09 g) were incorporated into the cellulose solution, followed by continuous stirring for 10 min and ultrasonication for 10 min. Then, 0.6 mL of the ECH was introduced into the mixture and stirred for an additional 30 min to ensure uniform dispersion. The resulting solution was transferred into molds and allowed to gel at room temperature for 2 h. Finally, the obtained hydrogels were immersed in a 2 mol L^{-1} LiCl aqueous solution for 24 h to yield ionic conductive cellulose hydrogels. During this process, the residual NaOH/urea was removed. The samples were labeled AS_0, $AS_{0.05}$, $AS_{0.1}$, and $AS_{0.15}$ when the ATS contents were of 0, 0.03, 0.06, and 0.09 g, respectively. For comparison, an ATP-reinforced hydrogel (denoted as $AP_{0.1}$) was prepared via the same method with 0.06 g of ATP instead of ATS.

Characterization. The morphology of the freeze-dried cellulose hydrogels was examined by scanning electron microscopy (SEM, Regulus 8100, Japan). X-ray diffraction (XRD) patterns were acquired on a Rigaku Ultima IV diffractometer with a scanning rate of 5° min^{-1} over a 2θ range of 5–50°. The rheological behavior of the hydrogels was investigated via a Rheowin MAS60 rheometer at ambient temperature, with oscillatory frequency sweeps performed from 0.1 to 100 rad s^{-1}. The cryoprotective properties were analyzed via differential scanning calorimetry (DSC, Netzsch DSC 200) under a nitrogen flow (20 mL min^{-1}), where the samples were cooled linearly

https://doi.org/10.1021/acs.langmuir.5c02530
Langmuir XXXX, XXX, XXX−XXX

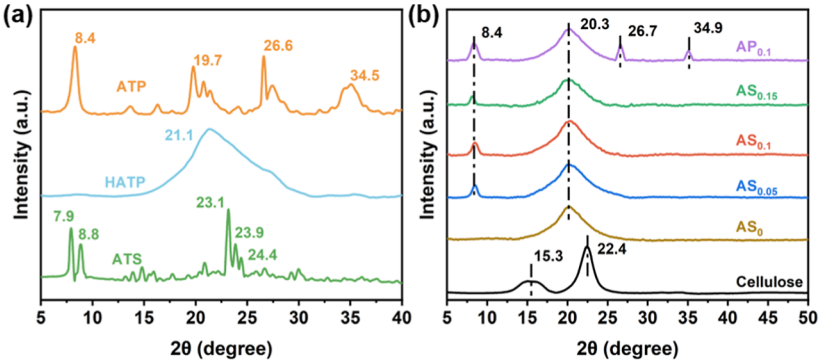

Figure 2. XRD patterns of the (a) original and modified ATP powders and (b) freeze-dried cellulose hydrogels and cellulose.

at 5 °C min^{-1} from −10 to −70 °C. The water retention capacity was evaluated under constant environmental conditions (25 °C, 50% relative humidity).

Mechanical Tests. The hydrogel tensile samples were prepared with a width of 13 mm and a thickness of 4.5 mm. Uniaxial tensile tests were performed at a constant strain rate of 10 mm min^{-1} via a universal testing machine (RH-5000N, Renheng Machinery Co., Ltd., Yangzhou, China). For compressive mechanical evaluation, cylindrical hydrogel samples with a diameter of 28 mm and a height of 17 mm were fabricated. The compressive tests were conducted under identical experimental conditions (strain rate: 10 mm min^{-1}) via the same testing system. All the measurements were repeated three times for each sample, and the average values were reported to ensure statistical reliability. The strain sensing performance of the hydrogel was characterized via an electrochemical workstation and an electronic universal testing machine. Copper foil electrodes affixed to both ends of the hydrogel served as electrical contacts. Resistance changes during tension/compression were recorded at a constant voltage of 1 V (details in the Supporting Information).

RESULTS AND DISCUSSION

Fabrication and Characterization of Cellulose Hydrogels. This study fabricated cellulose-based hydrogels by first dissolving cellulose in a NaOH/urea solution, subsequently incorporating inorganic ATS, chemically cross-linking with ECH, and finally immersing them in a LiCl solution.[27,28] By using TBOT as a Ti source, natural ATP was structurally reconstructed into ATS to serve as a hierarchical porous filler (Figure 1a). TBOT undergoes hydrolysis and reaction with silicate groups from ATP under hydrothermal conditions, forming Si−O−Ti bonds. Cotton linters, employed as the cellulose source, were dispersed in an aqueous NaOH/urea solution.[29] The resulting cellulose solution was homogeneously blended with ATS particles to form a uniform suspension. ECH, which acts as a chemical cross-linker, was subsequently introduced into the hydrogel matrix.[30] Covalent cross-linking between cellulose chains and ECH via ether linkages established a robust chemically cross-linked network (Figure 1b). Concurrently, ATS particles interact with cellulose chains through hydrogen bonding, forming a secondary physically cross-linked network that significantly accelerates gelation kinetics. The integration of ATSs not only refined the hydrogel architecture by modulating the spatial arrangement of cellulose networks but also leveraged its well-defined porosity to facilitate rapid ion transport.[31]

XRD pattern of the original ATP samples (Figure 2a) exhibits characteristic diffraction peaks at 8.4°, 19.7°, 26.6°, and 34.5°.[32] After HCl treatment, these distinct peaks vanished, and a broad diffraction peak emerged at ca. 21.1° for HATP, indicating the transformation of the crystalline structure into an amorphous silica matrix composed of disordered Si tetrahedral chains. Notably, the XRD pattern of ATS reveals peaks at 7.9°, 8.8°, 23.1°, 23.9°, and 24.4°, which are indexed to the (101), (200), (501), (303), and (313) planes of MFI-type titanosilicate molecular sieves. This confirms the successful synthesis of ATS. The crystal structures of the pristine cellulose and freeze-dried cellulose hydrogels were analyzed via XRD (Figure 2b). Pristine cellulose displays characteristic peaks at 15.3° and 22.4°, corresponding to its native type I crystalline phase.[33] Upon dissolution in the NaOH/urea system and subsequent hydrogel formation, these peaks shifted, indicating a structural transition to type II cellulose with reduced crystallinity due to hydrogen bond disruption and chain realignment.[34]

The morphological evolution during ATP-to-ATS conversion was investigated via SEM (Figure 3a and b). Raw

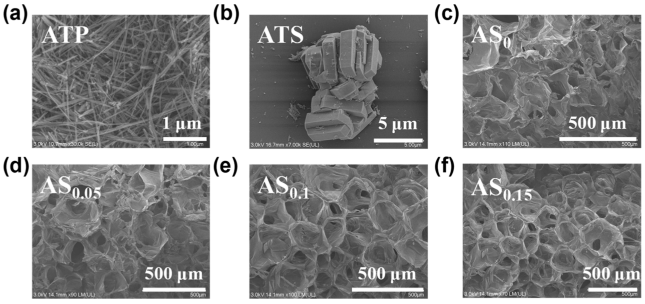

Figure 3. SEM images of (a) raw ATP, (b) ATS and (c−f) freeze-dried cellulose gels with different ATS contents.

ATP has a rod-like morphology (about 20−40 nm in diameter), whereas post-treatment ATS has a micrometer-sized particulate structure. Freeze-dried hydrogels (Figure 3c−f) display an interconnected porous architecture, where increasing the ATS content reflects the pore uniformity and density. This hierarchical porosity is expected to facilitate ion transport and enhance the mechanical performance.[15]

As shown in Figure 4a, the as-prepared hydrogel ($AS_{0.1}$) exhibited remarkable flexibility, maintaining structural integrity without rupture even under severe twisting and folding deformation. This indicates the high toughness and shape-recovery capability of the composite hydrogel. Tensile tests were conducted to evaluate the mechanical properties (Figure 4b). The pristine hydrogel (AS_0), governed by strong hydrogen bonding between cellulose chains, formed a densely entangled network with inherent brittleness, resulting in inferior mechanical strength (56 kPa tensile strength) and

https://doi.org/10.1021/acs.langmuir.5c02530
Langmuir XXXX, XXX, XXX−XXX

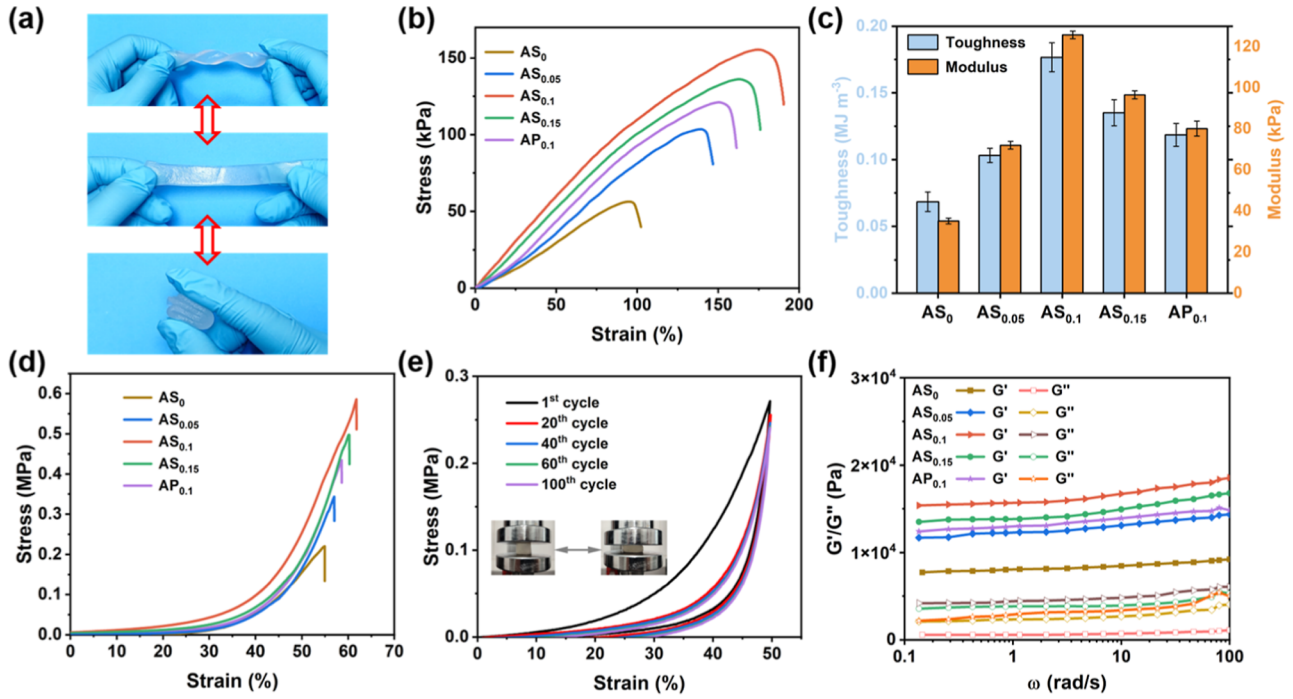

Figure 4. (a) Photographs showing the flexibility and robustness of $AS_{0.1}$ at room temperature. (b) Tensile stress−strain curves, (c) modulus of elasticity and toughness, and (d) compressive stress−strain curves of ATS/cellulose hydrogels. (e) Compression cyclic stress−strain curves of $AS_{0.1}$ at 50% strain. (f) Rheological properties of the cellulose hydrogels.

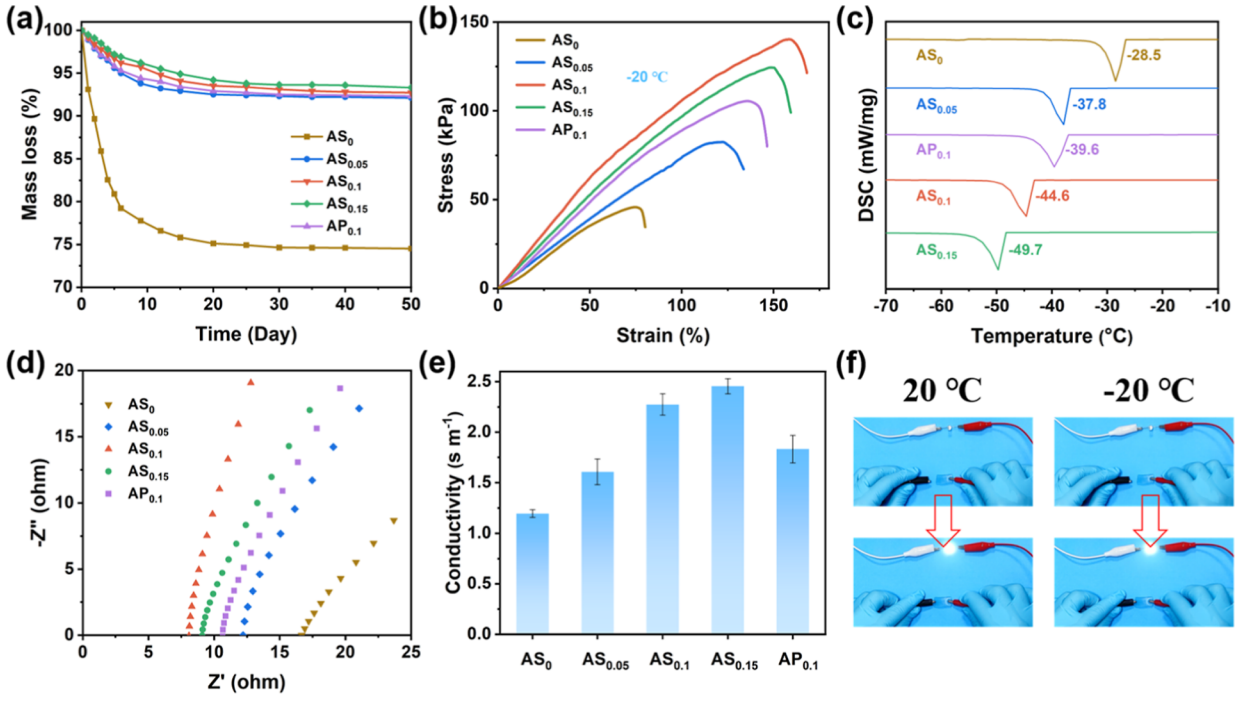

Figure 5. (a) Water retention curves, (b) low-temperature tensile stress−strain curves, (c) DSC curves, (d) EIS curves, and (e) ionic conductivities of the cellulose hydrogels. (f) Images of $AS_{0.1}$ used as conductors at different temperatures.

limited ductility (96% elongation at break).[35] In contrast, the incorporation of ATS significantly enhanced the performance of the hydrogel. The tensile strength of the optimal sample ($AS_{0.1}$) reached 155 kPa, and the elongation at break was 177%, representing 176% and 84% improvements over AS_0, respectively. This enhancement stems from the dual-cross-linked network, e.g., the primary covalent network formed by ECH ensures structural stability, whereas the secondary physical network formed via ATS-cellulose hydrogen bonding enables efficient energy dissipation.[36] The tensile cyclic stress−strain curves of $AS_{0.1}$ at 100% strain were determined (Figure S1, Supporting Information). The hysteresis curves are well-maintained after 100 continuous loading−unloading cycles, indicating its good shape recovery capability.

https://doi.org/10.1021/acs.langmuir.5c02530
Langmuir XXXX, XXX, XXX−XXX

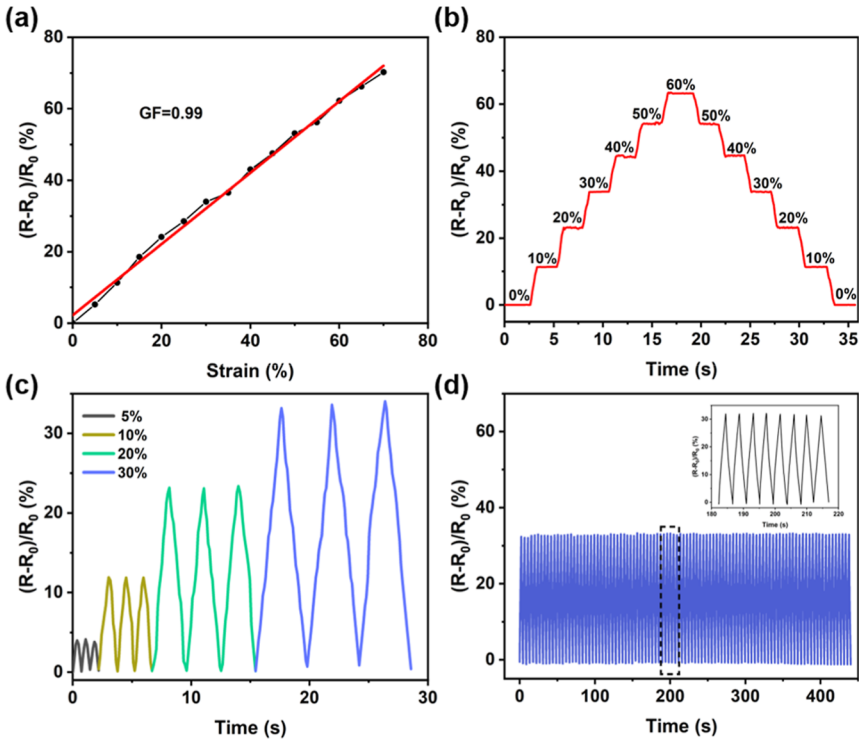

Figure 6. (a) Variation in the relative resistance with tensile strain, (b) relative resistance curve changes under a tensile strain from 0 to 60%, (c) relative resistance change under different cyclic tensile strains, and (d) relative resistance change for 100 cycles of loading−unloading at 30% strain tested on the $AS_{0.1}$ sample.

Notably, $AS_{0.1}$ outperformed the ATP-based counterpart ($AP_{0.1}$), highlighting the critical role of ATS in reinforcing mechanical robustness. Both the tensile strength and elongation at break increased proportionally with the ATS content (Figure 4c). $AS_{0.1}$ exhibited the highest elastic modulus (125 kPa) and toughness (0.17 MJ m^{-3}), which was attributed to the stress distribution effect of the ATS-induced secondary network. Acid-hydrothermal modification converts native ATP irregular rods into ATS particles with hierarchical porosity. This uniform structure provides abundant sites for strong hydrogen bonding with cellulose chains. However, high ATS loading (e.g., $AS_{0.15}$) induced particle aggregation, disrupting stress homogeneity and compromising mechanical integrity.[37]

The compression tests further revealed the role of the ATS in enhancing the load-bearing capacity (Figure 4d). The pristine hydrogel (AS_0) displayed a modest compressive stress of 0.22 MPa, whereas $AS_{0.1}$ reached 0.58 MPa. The signal in tension is more sensitive than that at the compression state. Cyclic compression at 50% strain over 100 cycles (Figure 4e) confirmed the durability of the hydrogel. The emergence of hysteresis loops after 20 cycles indicated reversible hydrogen bond breakage and reformation, ensuring elasticity and fatigue resistance.[38,39] The rheological analysis in Figure 4f corroborated the structural stability, as the storage modulus (G') consistently exceeded the loss modulus (G'') across the tested frequency range (0.1−100 rad s^{-1}), which is characteristic of a covalently cross-linked elastic hydrogel. The frequency-independent moduli further affirmed the robustness of the dual-network architecture.[40]

Water loss under ambient conditions remains a critical challenge for hydrogels, as dehydration severely compromises their structural integrity and functional performance. To evaluate the water retention capability, Figure 5a shows that the pristine cellulose hydrogel (AS_0) retained only 74% of its initial weight after 50 days under constant conditions (25 °C, 50% RH), whereas the ATS-reinforced hydrogels preserved more than 92% of their original mass. The rapid initial dehydration followed by a gradual decline in water loss can be attributed to the presence of hydrophilic hydroxyl groups on both the cellulose and ATS surfaces, which stabilize water molecules via hydrogen bonding. In addition, freezing tolerance is a vital property for low-temperature applications. The ATS-incorporated hydrogel ($AS_{0.1}$) retained 90% of its tensile strength after 48 h at −20 °C (Figure 5b), confirming its exceptional frost resistance. The DSC analysis results (Figure 5c) revealed a decrease in freezing points from −28.5 °C (pristine hydrogel) to −44.6 °C ($AS_{0.1}$). This is attributable to two synergistic mechanisms: (i) the increased cross-linking density induced by ATS restricts ice crystal nucleation, and (ii) LiCl addition disrupts hydrogen-bonded water networks via ion−dipole interactions.[19,41]

The porous architecture of the hydrogel, combined with abundant LiCl ions, facilitates efficient ion transport. EIS analysis (Figure 5d) revealed a bulk resistance-derived ionic conductivity of 1.19 S m^{-1} for AS_0, which increased to 2.45 S m^{-1} for ATS-incorporated $AS_{0.1}$ (Figure 5e). This enhancement stems from ATS-mediated structural optimization, whereas the dense hydrogen-bonded network of pristine cellulose hinders ion diffusion. Notably, the ATP-modified counterpart ($AP_{0.1}$) exhibited inferior conductivity (1.83 S m^{-1}), confirming the superiority of ATSs in tailoring ion channels.[42] The $AS_{0.1}$ hydrogel was compared with other hydrogels reported in the literature (Table S1, Supporting Information). Practical validation via circuit connectivity tests (Figure 5f) revealed that the hydrogel has robust low-

https://doi.org/10.1021/acs.langmuir.5c02530
Langmuir XXXX, XXX, XXX−XXX

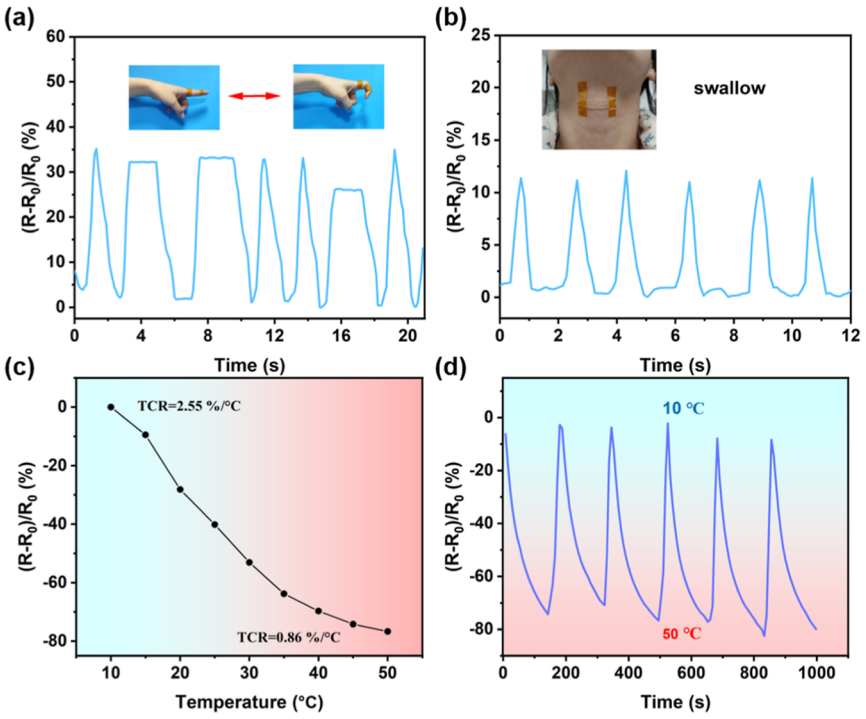

Figure 7. (a,b) Cellulose hydrogel as a sensor to detect human movement, finger flexion, and throat swallowing. (c) Relative resistance curve of the $AS_{0.1}$ hydrogel as a function of temperature. (d) Changes in the relative resistance of the $AS_{0.1}$ hydrogels over 10−50 °C cycles.

temperature performance. After storing at −20 °C for 12 h, the $AS_{0.1}$ hydrogel maintained continuous illumination with a slight luminance reduction as compared to that at 20 °C. The ATS-enhanced cross-linking density restricts ice nucleation, preserving ion-transport channels and enabling continuous ion hopping through ATS-engineered porous pathways.

Sensing Performance. Owing to their superior mechanical robustness and ionic conductivity, ATS/cellulose hydrogels have promising potential as sensors. To evaluate the sensing capabilities of $AS_{0.1}$. A sensor was fabricated by sandwiching a hydrogel between two copper electrodes. Under tensile deformation, a hydrogel undergoes geometric changes in length and cross-sectional area, thereby modulating its electrical resistance. The sensitivity to strain was quantified via the gauge factor (GF), which is defined as the ratio of the relative resistance change $\Delta R/R_0$ to the applied strain (ε). A linear correlation between $\Delta R/R_0$ and ε was observed across varying strains, yielding a gauge factor (GF) of 0.99 (Figure 6a).

Systematic tensile testing revealed a progressive increase in the relative resistance as $AS_{0.1}$ was gradually stretched from 0% to 60% strain (Figure 6b), confirming its strain-responsive behavior. Notably, the hydrogel exhibited stable and repeatable signal output under low-strain conditions (Figure 6c). The observed resistance increase under stretching originates from the elongation of ionic transport pathways within the hydrogel network. As the polymer chains are stretched, the tortuosity of the ion migration routes increases, increasing the charge transfer resistance and consequently increasing ($\Delta R/R_0$).[43] Fatigue resistance, a key metric for sensor durability, was validated through 100 consecutive loading−unloading cycles at 30% strain, during which the hydrogel maintained consistent electrical responses without signal degradation (Figure 6d). Similarly, compression tests were conducted, and the $AS_{0.1}$ sample exhibited good sensitivity and fatigue resistance (Figure S2, Supporting Information). The dual-network design ensures efficient stress dissipation and structural recovery, which are critical for sustained sensing accuracy under repeated mechanical stimuli.[44]

The ATS/cellulose hydrogel was engineered into a wearable motion sensor for real-time detection of human physiological activities. To validate its functionality, the optimized hydrogel ($AS_{0.1}$) was integrated with copper electrodes and secured to volunteer anatomical sites (elbow, wrist, finger, and throat) through medical-grade adhesive tape (Figures 7a and S3, Supporting Information). The sensor demonstrated robust tracking of motion-induced electrochemical signal variations with millisecond-level temporal resolution (Figure 7b).

Temperature-dependent conductivity analysis revealed a monotonic decrease in the relative resistance ($\Delta R/R_0$) as the temperature increased from 10 to 50 °C (Figure 7c). The temperature coefficient of resistance (TCR) is calculated as $(\Delta R/R_0)/\Delta T$. The $AS_{0.1}$ hydrogel has a sensitive TCR value of 2.55% $°C^{1-}$ in the range of 10 to 30 °C and 0.86% $°C^{1-}$ in the range of 30 to 50 °C. Thermal cycling tests (10−50 °C) confirmed reversible resistance modulation (Figure 7d). The enhanced ionic conductivity of hydrogels at elevated temperatures can be attributed to thermally activated ion transport dynamics.[45]

CONCLUSION

In this work, a novel fabrication strategy was developed to prepare high-strength, freeze-resistant cellulose-based conductive hydrogels. The dual-network architecture comprising covalent cross-links and hydrogen-bonded interfaces synergistically enhanced the mechanical resilience by dissipating stress concentrations while simultaneously optimizing the ionic conductivity. The optimal hydrogel ($AS_{0.1}$) achieves a tensile strength of 155 kPa and a compressive stress of 0.58 MPa. Simultaneously, the ATS-engineered porous network facilitates

https://doi.org/10.1021/acs.langmuir.5c02530
Langmuir XXXX, XXX, XXX−XXX

rapid ion transport, yielding a high ionic conductivity of 2.45 S m^{-1}. $AS_{0.1}$ demonstrated high sensitivity to both large-scale motions (e.g., elbow/wrist flexion) and subtle physiological activities (e.g., throat swallowing), achieving millisecond-level response times and good stability. This work not only provides a green strategy for high-performance hydrogels but also elucidates the structure−property relationships between inorganic fillers and polymer networks, offering insights for designing next-generation biobased sensors.

■ ASSOCIATED CONTENT

Supporting Information

The Supporting Information is available free of charge at https://pubs.acs.org/doi/10.1021/acs.langmuir.5c02530.

All experiments were conducted in accordance with the Electrochemical measurements; Sensing performance evaluation; Tensile stress−strain curves of $AS_{0.1}$ at 100% strain for 100 loading−unloading cycles (Figure S1); The compressive sensing performance of $AS_{0.1}$ hydrogel (Figure. S2); $AS_{0.1}$ hydrogel as a sensor to detect human movement: elbow flexion/extension and wrist flexion (Figure. S3); Comparison of $AS_{0.1}$ hydrogel with other hydrogels (Table S1) (PDF)

■ AUTHOR INFORMATION

Corresponding Authors

Xiong-Fei Zhang − *Jiangsu Co-Innovation Center of Efficient Processing and Utilization of Forest Resources, College of Chemical Engineering, Nanjing Forestry University, Nanjing 210037, China*; Email: zxf1990@njfu.edu.cn

Jianfeng Yao − *Jiangsu Co-Innovation Center of Efficient Processing and Utilization of Forest Resources, College of Chemical Engineering, Nanjing Forestry University, Nanjing 210037, China*; orcid.org/0000-0002-3619-6741; Email: jfyao@njfu.edu.cn

Authors

Miaomiao Wu − *Jiangsu Co-Innovation Center of Efficient Processing and Utilization of Forest Resources, College of Chemical Engineering, Nanjing Forestry University, Nanjing 210037, China*

Hu Liu − *Jiangsu Co-Innovation Center of Efficient Processing and Utilization of Forest Resources, College of Chemical Engineering, Nanjing Forestry University, Nanjing 210037, China*

Mengjie Li − *Jiangsu Co-Innovation Center of Efficient Processing and Utilization of Forest Resources, College of Chemical Engineering, Nanjing Forestry University, Nanjing 210037, China*

Complete contact information is available at: https://pubs.acs.org/10.1021/acs.langmuir.5c02530

Notes

Declaration of Helsinki. Informed consent was obtained from all participants prior to their inclusion in the study.

The authors declare no competing financial interest.

■ ACKNOWLEDGMENTS

The authors are grateful for financial support from the National Natural Science Foundation of China (52103113), Qinglan Project of Jiangsu Province (Su-2024Y05) and the Forestry Science and Technology Innovation and Extension Project of Jiangsu Province (LYKJ [2021] 04).

■ REFERENCES

(1) Zhang, Y.; Tan, Y.; Lao, J.; Gao, H.; Yu, J. Hydrogels for Flexible Electronics. *ACS Nano* **2023**, *17* (11), 9681−9693.

(2) Hu, L.; Chee, P. L.; Sugiarto, S.; Yu, Y.; Shi, C.; Yan, R.; Yao, Z.; Shi, X.; Zhi, J.; Kai, D.; Yu, H. D.; Huang, W. Hydrogel-Based Flexible Electronics. *Adv. Mater.* **2023**, *35* (14), 2205326.

(3) Li, Y.; Liu, L.; Zhao, C.; Guo, M.; Wu, Y.; Chen, S.; Cheng, J.; Xiang, D.; Li, H.; Wang, L. Multifunctional double network hydrogel with multi-directional actuation and high-precision sensing. *Sens. Actuators, B* **2025**, *422*, 136669.

(4) Tang, J.; Gou, K.; Wang, C.; Wei, M.; Tan, Q.; Weng, G. Self-Powered and 3D printable soft sensor for human health monitoring, object recognition, and contactless hand gesture recognition. *Adv. Funct. Mater.* **2024**, *34* (52), 2411172.

(5) Jia, L.; Jiang, J.; Ren, A.; Wei, Z.; Xiang, T.; Zhou, S. Ultra-fast cryogenic self-healing ionic hydrogel for flexible wearable bioelectronics. *Chem. Eng. J.* **2024**, *495*, 153734.

(6) Wang, Y.; Zhang, Y.; Ren, P.; Yu, S.; Cui, P.; Nielsen, C. B.; Abrahams, I.; Briscoe, J.; Lu, Y. Versatile and recyclable double-network PVA/cellulose hydrogels for strain sensors and triboelectric nanogenerators under harsh conditions. *Nano Energy* **2024**, *125*, 109599.

(7) Huang, J.; Zhao, L.; Xiang, P.; Zhang, F.; Yang, Y.; Chao, L.; Liu, W.; Li, H.; Zhang, X. Aminated lignin/cellulose-based hydrogel with high adhesion for wearable sensors. *Langmuir* **2025**, *41* (24), 15484−15493.

(8) Zhao, R.; Zhao, Z.; Song, S.; Wang, Y. Multifunctional Conductive Double-Network Hydrogel Sensors for Multiscale Motion Detection and Temperature Monitoring. *ACS Appl. Mater. Interfaces* **2023**, *15* (51), 59854−59865.

(9) Wang, M.; Li, L.; Zhang, T. Hysteresis-free, fatigue-resistant and self-adhesive conductive hydrogel electronics towards multimodal wearable application. *Nano Energy* **2024**, *126*, 109586.

(10) Ge, G.; Zhang, Y.; Shao, J.; Wang, W.; Si, W.; Huang, W.; Dong, X. Stretchable, Transparent, and Self-Patterned Hydrogel-Based Pressure Sensor for Human Motions Detection. *Adv. Funct. Mater.* **2018**, *28* (32), 1802576.

(11) Zhao, D.; Huang, J.; Zhong, Y.; Li, K.; Zhang, L.; Cai, J. High-Strength and High-Toughness Double-Cross-Linked Cellulose Hydrogels: A New Strategy Using Sequential Chemical and Physical Cross-Linking. *Adv. Funct. Mater.* **2016**, *26* (34), 6279−6287.

(12) Zhang, Y.; Chen, M.; Lu, J.; Ma, H.; Liu, W.; Yu, J.; Tian, Q.; Xu, J.; Chen, J. Anisotropic and anti-freezing cellulose hydrogel electrolyte with aligned channels stabilizing Zn metal anode. *Chem. Eng. J.* **2025**, *506*, 159950.

(13) Zhou, H.; Lai, J.; Jin, X.; Liu, H.; Li, X.; Chen, W.; Ma, A.; Zhou, X. Intrinsically adhesive, highly sensitive and temperature tolerant flexible sensors based on double network organohydrogels. *Chem. Eng. J.* **2021**, *413*, 127544.

(14) Wei, D.; Lv, S.; Zuo, J.; Liu, J.; Wang, J.; Liu, L.; Zeng, Q. Engineering versatile bi-network ionic conductive hydrogels wearable sensors via on demand graft modification for real-time human movement monitoring. *Chem. Eng. J.* **2024**, *496*, 154176.

(15) Hu, S.; Huang, Y.; Liu, X.; Zong, C.; Lei, L.; Li, H. Mechanically robust and highly conductive bacterial cellulose hydrogels through synergy of directional freeze−thawing and salting-out for wearable sensors. *Chem. Eng. J.* **2024**, *499*, 156161.

(16) Wang, Y.; Zhang, L.; Lu, A. Highly stretchable, transparent cellulose/PVA composite hydrogel for multiple sensing and triboelectric nanogenerators. *J. Mater. Chem. A* **2020**, *8* (28), 13935−13941.

(17) Wang, Z.; Zhou, Z.; Wang, S.; Yao, X.; Han, X.; Cao, W.; Pu, J. An anti-freezing and strong wood-derived hydrogel for high-performance electronic skin and wearable sensing. *Composites, Part B.* **2022**, *239*, 109954.

(18) Wang, S.; Yu, L.; Wang, S.; Zhang, L.; Chen, L.; Xu, X.; Song, Z.; Liu, H.; Chen, C. Strong, tough, ionic conductive, and freezing-tolerant all-natural hydrogel enabled by cellulose-bentonite coordination interactions. *Nat. Commun.* **2022**, *13* (1), 3408.
(19) Liu, H.; Zhang, X.-F.; Li, M.; Yao, J. Attapulgite-Reinforced Cellulose Hydrogels with High Conductivity and Antifreezing Property for Flexible Sensors. *Langmuir* **2024**, *40* (40), 20986−20994.
(20) Zhou, X.; Liu, Y.; Meng, X.; Shen, B.; Xiao, F.-S. Synthesis and catalytic cracking performance of Fe/Ti-ZSM-5 zeolite from attapulgite mineral. *Chin. J. Catal.* **2013**, *34* (8), 1504−1512.
(21) Feng, M.; Kou, Z.; Tang, C.; Shi, Z.; Tong, Y.; Zhang, K. Recent progress in synthesis of zeolite from natural clay. *Appl. Clay Sci.* **2023**, *243*, 107087.
(22) Jing, X.; Li, H.; Mi, H.-Y.; Liu, Y.-J.; Feng, P.-Y.; Tan, Y.-M.; Turng, L.-S. Highly transparent, stretchable, and rapid self-healing polyvinyl alcohol/cellulose nanofibril hydrogel sensors for sensitive pressure sensing and human motion detection. *Sens. Actuators, B* **2019**, *295*, 159−167.
(23) Fu, D.; Yang, R.; Wang, R.; Wang, Y.; Li, Y.; Bian, H. A triple-crosslinked, self-healing, polyvinyl alcohol/nanocellulose hydrogel for versatile sensing applications. *Carbohydr. Polym.* **2024**, *334*, 122060.
(24) Binder, S.; Gerlach, G. Performance of force-compensated chemical sensors based on bisensitive hydrogels. *Sens. Actuators, B* **2021**, *342*, 129420.
(25) Xi, Y.; Zhang, L.; Tian, Y.; Song, J.; Ma, J.; Wang, Z. Rapid dissolution of cellulose in an AlCl3/ZnCl2 aqueous system at room temperature and its versatile adaptability in functional materials. *Green Chem.* **2022**, *24* (2), 885−897.
(26) Wang, Y.; Shen, L.; Liang, D.; Yao, J.; Chen, C.; Chen, M.; Xin, H.; Li, C. Attapulgite-based titanosilicate zeolite-supported Ni catalyst for hydrogen production from catalytic steam reforming of toluene. *J. Anal. Appl. Pyrolysis* **2024**, *177*, 106297.
(27) Cai, J.; Zhang, L. Rapid Dissolution of Cellulose in LiOH/Urea and NaOH/Urea Aqueous Solutions. *Macromol. Biosci.* **2005**, *5* (6), 539−548.
(28) Wang, Z.; Zhang, X.-F.; Shu, L.; Yao, J. Copper sulfide integrated functional cellulose hydrogel for efficient solar water purification. *Carbohydr. Polym.* **2023**, *319*, 121161.
(29) Jiang, Z.; Fang, Y.; Xiang, J.; Ma, Y.; Lu, A.; Kang, H.; Huang, Y.; Guo, H.; Liu, R.; Zhang, L. Intermolecular Interactions and 3D Structure in Cellulose-NaOH-Urea Aqueous System. *J. Phys. Chem. B* **2014**, *118* (34), 10250−10257.
(30) Palanivelu, S. D.; Gan, S.; Salleh, K. M.; Lindsey, K.; Sairi, F.; Che-Othman, M. H.; Zakaria, S. Assessment of bio-based hydrogel as an alternative growth medium for seed germination and seedling growth in urban farming. *Cellulose* **2023**, *30* (12), 7791−7803.
(31) Ye, Y.; Yu, L.; Lizundia, E.; Zhu, Y.; Chen, C.; Jiang, F. Cellulose-Based Ionic Conductor: An Emerging Material toward Sustainable Devices. *Chem. Rev.* **2023**, *123* (15), 9204−9264.
(32) Liu, Y.; Liu, Y.; Niu, Y.; Qu, R. Fast and highly efficient removal of organic dyes from aqueous solution by attapulgite modified with different amino groups. *Colloid Surf. A* **2024**, *687*, 133543.
(33) Zhang, L.; Zhou, J.; Zhang, L. Structure and properties of β-cyclodextrin/cellulose hydrogels prepared in NaOH/urea aqueous solution. *Carbohydr. Polym.* **2013**, *94* (1), 386−393.
(34) Miao, H.; Liu, Y.; Zheng, C.; Huang, X.; Song, Y.; Tong, L.; Dong, C.; Fu, X.; Huang, H.; Ge, M.; Liu, H.; Qian, Y. A flexible, antifreezing, and long-term stable cellulose ionic conductive hydrogel via one-step preparation for flexible electronic sensors. *Carbohydr. Polym.* **2025**, *351*, 122936.
(35) Tian, Y.; Zhang, L.; Li, X.; Yan, M.; Wang, Y.; Ma, J.; Wang, Z. Compressible, anti-freezing, and ionic conductive cellulose/poly-acrylic acid composite hydrogel prepared via $AlCl_3/ZnCl_2$ aqueous system as solvent and catalyst. *Int. J. Biol. Macromol.* **2023**, *253*, 126550.
(36) Xia, Q.; Li, W.; Zou, X.; Zheng, S.; Liu, Z.; Li, L.; Yan, F. Metal−organic framework (MOF) facilitated highly stretchable and fatigue-resistant ionogels for recyclable sensors. *Mater. Horiz.* **2022**, *9* (11), 2881−2892.
(37) Guo, C.; Zhu, A.; Wang, X.; Dai, J.; Luo, L.; Xu, Y.; Zeng, B.; Chen, G.; Dai, L. Ultra-stretchable and anti-freezing conductive organohydrogel reinforced with ionic clusters for wearable strain sensors. *Sens. Actuators, B* **2022**, *362*, 131796.
(38) Li, J.; Chen, F.; Lin, X.; Ding, T. Hydrogen-bonding-assisted toughening of hierarchical carboxymethyl cellulose hydrogels for biomechanical sensing. *Carbohydr. Polym.* **2021**, *269*, 118252.
(39) Li, W.; Li, L.; Zheng, S.; Liu, Z.; Zou, X.; Sun, Z.; Guo, J.; Yan, F. Recyclable, Healable, and Tough Ionogels Insensitive to Crack Propagation. *Adv. Mater.* **2022**, *34* (28), 2203049.
(40) Li, X.; Wang, Y.; Tian, Y.; Zhang, L.; Ma, J. Biomimetic multiscale structure with hierarchically entangled topologies of cellulose-based hydrogel sensors for human-computer interaction. *Carbohydr. Polym.* **2025**, *348*, 122825.
(41) Zhang, X. F.; Ma, X.; Hou, T.; Guo, K.; Yin, J.; Wang, Z.; Shu, L.; He, M.; Yao, J. Inorganic Salts Induce Thermally Reversible and Anti-Freezing Cellulose Hydrogels. *Angew. Chem., Int. Ed.* **2019**, *58* (22), 7366−7370.
(42) Pérez-Mitta, G.; Toimil-Molares, M. E.; Trautmann, C.; Marmisollé, W. A.; Azzaroni, O. Molecular Design of Solid-State Nanopores: Fundamental Concepts and Applications. *Adv. Mater.* **2019**, *31* (37), 1901483.
(43) Hu, K.; Zhao, Z.; Wang, Y.; Yu, L.; Liu, K.; Wu, H.; Huang, L.; Chen, L.; Ni, Y. A tough organohydrogel-based multiresponsive sensor for a triboelectric nanogenerator and supercapacitor toward wearable intelligent devices. *J. Mater. Chem. A* **2022**, *10* (22), 12092−12103.
(44) Yang, L.; Liu, Q.; Li, M.; Liu, Y.; Li, X.; Liu, Q.; Zhu, T.; Lu, Y.; Liu, X.; Wang, D. A high-performance, flexible, and dual-modal humidity-piezoelectric sensor without mutual interference. *Sens. Actuators, B* **2025**, *423*, 136778.
(45) Wu, Y.; Zhang, X.-F.; Li, M.; Yu, M.; Yao, J. Self-Healing and Wide Temperature-Tolerant Cellulose-Based Eutectogels for Reversible Humidity Detection. *Langmuir* **2024**, *40* (10), 5288−5296.

https://doi.org/10.1021/acs.langmuir.5c02530
Langmuir XXXX, XXX, XXX−XXX